Cold-air Bypass Characterization for Fuel Cell Thermal Management in Fuel Cell Turbine Hybrids

Valentina Zaccaria, David Tucker, Alberto Traverso

Cold-air Bypass Characterization for Fuel Cell Thermal Management in Fuel Cell Turbine Hybrids

Valentina Zaccaria[1]*, David Tucker[1], Alberto Traverso[2]

ISROMAC 2016

International Symposium on Transport Phenomena and Dynamics of Rotating Machinery

Hawaii, Honolulu

April 10-15, 2016

Abstract

The effect of cathode airflow variation on the dynamics of a fuel cell gas turbine hybrid system was evaluated using a cyber-physical emulator. The coupling between cathode airflow and other parameters, such as turbine speed or pressure, was analyzed comparing the results at fixed and variable speed. In particular, attention was focused on the fuel cell temperatures, since cathode airflow is generally employed for thermal management of the stack. A significant difference was observed in the two cases in terms of turbine inlet, exhaust gas, cathode inlet, and average cell temperatures. When the turbine speed was held constant, a change in cathode airflow resulted in a strong variation in cathode inlet temperature, while average cell temperature was not significantly affected. The opposite behavior was observed at variable speed. The system dynamics were analyzed in details in order to explain this difference. Open loop response was analyzed in this work for its essential role in control systems development. But, the significant difference shown in this work proved that some trends are not adequately captured with a standard system identification procedure, because of the high coupling between turbine speed and cathode airflow. Cold air valve bypass position also showed a strong impact on surge margin in both cases.

Keywords

Fuel cell hybrids — Cyber-physical simulation — Cathode airflow

[1] *U.S. Department of Energy, National Energy Technology Laboratory, Morgantown, WV, United States*

[2] *Thermochemical Power Group, University of Genova, Genova, Italy*

*__Corresponding author__: valentina.zaccaria@netl.doe.gov

INTRODUCTION

The hybridization of high temperature fuel cell and gas turbine facilitates very high efficiency, increased system flexibility, and extended fuel cell component lifetime [1-5]. Recovering the waste heat from the fuel cell with a gas turbine, it is possible to enhance the power production and use the compressor to pressurize the fuel cell at no additional cost, reaching efficiency levels that are not possible with the separate technologies [3]. However, the interaction between the two coupled systems presents new significant challenges in terms of controls. In a hybrid system different variables, for instance turbine speed and cathode airflow, are strongly coupled, i.e. a change in one variable affects the second one and vice-versa. In addition, the time response of the two main components, fuel cell and gas turbine, are substantially different [6]. These aspects result in more complicated control of the system.

There are only a few hardware-based facilities in the world designed to study the coupling of a gas turbine and a solid oxide fuel cell, and the associated control issues [7, 8]. The Hybrid Performance (HyPer) facility, located in the U.S. Department of Energy, National Energy Technology Laboratory, is the only one designed to evaluate high speed dynamic phenomena in hybrid systems. The facility matches hardware and virtual components to take advantages from model flexibility and experimental accuracy [9].

In order to ensure safe operability and optimize the system efficiency, the characterization of the different actuators was performed on the HyPer facility with the final goal of implementing control systems capable of facing the new challenges [10-14]. In particular, cathode airflow management was considered extremely important to keep cell temperature and temperature gradients in a safe range [15], but its variation showed to affect several other parameters in the system, such as turbine speed, pressure, and surge margin [11, 13, 16]. In previous works the system response to a variation in cathode airflow was evaluated in an open loop configuration, where no control action was applied to regulate turbine speed or turbine inlet temperature [13, 17]. In these works, cathode airflow was changed via manipulating a hot air bypass, and the coupling between airflow and turbine speed was shown when the fuel cell model was in the loop. The non-linear behavior of some of the actuators was also investigated without the real-time simulation driving the system [11, 12]. A complete characterization of these actuators was considered very important to study possible control actions. In this work, the impact of cathode airflow variation on the system dynamics was studied comparing two different scenarios: in the first case turbine speed was free to change (open loop configuration), in the second one it was kept constant via manipulating the electric load imposed to the turbine (closed loop configuration).

Open loop tests are useful to study the transient dynamics of the system, but the system response when the speed is controlled is also important since it represents a realistic plant configuration. System identification in closed loop can give a more insight knowledge of the system dynamics. A more complete system identification helps to develop accurate control strategies.

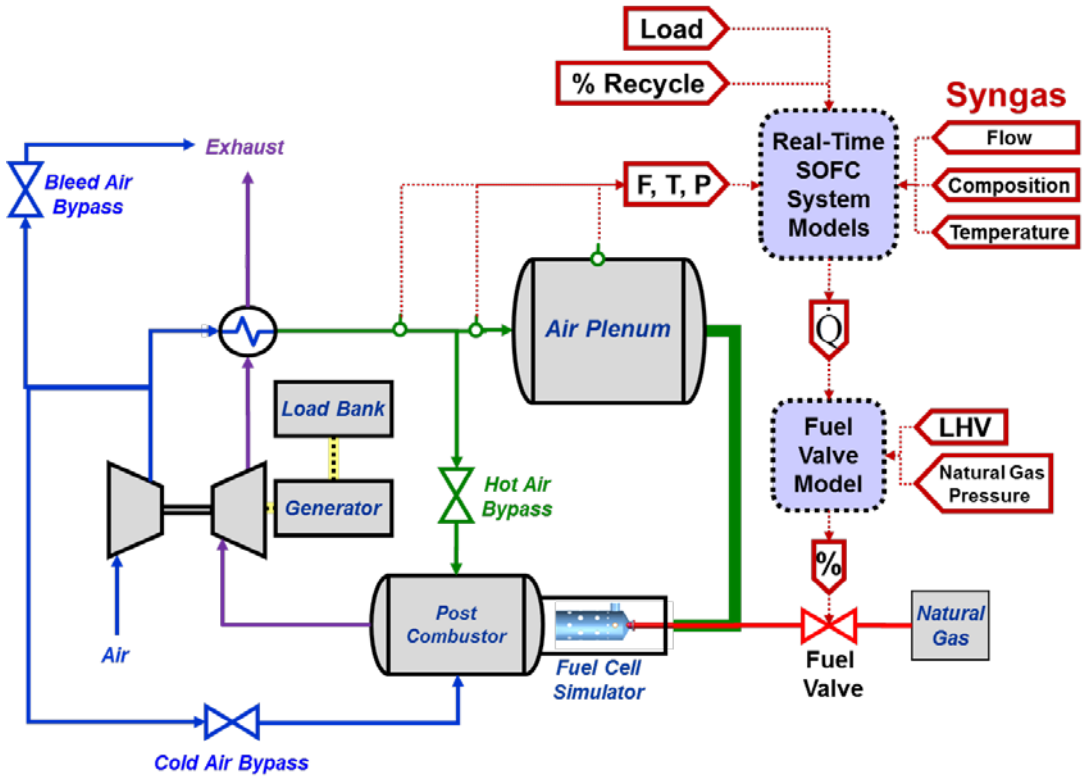

Figure 1. Hyper facility schematic diagram

NOMENCLATURE

h	specific enthalpy variation from 298 K reference condition [kJ/kg]
$\dot{m}$	mass flow rate [kg/s]
$\dot{m}_{nd}$	non-dimensional mass flow rate
PID	Proportional Integrative Derivative
$\dot{Q}$	transferred heat [kW]
SM	Surge Margin
SOFC	Solid Oxide Fuel Cell
TIT	Turbine Inlet Temperature
TOT	Turbine Outlet Temperature
β	pressure ratio
Δ	difference

1. FACILITY DESCRIPTION

Two experiments were carried out using a cyber-physical simulation approach. In this approach the hardware components of the HyPer facility were coupled with a numerical real-time model of a solid oxide fuel cell (SOFC), which drove the only heat source of the system. The hardware components of the fuel cell emulator included a natural gas combustor to simulate the heat from the fuel cell and two vessels to emulate the volumes of the fuel cell system, and they were physically coupled to a recuperated gas turbine.

A schematic representation of the plant is presented in Figure 1, where all the dash lines represent the numerical model. The model also includes a dynamic module of a biomass gasifier, not included in this work [18].

The compressed air was preheated by the turbine exhaust into the two counter-flow heat exchangers, before feeding the cathode and air manifold volumes emulator, which consisted of a pressurized vessel. Here the pressure dynamics of the fuel cell were simulated. After the volume, a natural gas combustor generated the amount of heat calculated in the fuel cell model, which was used to drive a 120 kW turbine. A second vessel was located after the combustor to simulate the volume of the post-combustor in the fuel cell system.

Three bypass valves were used for control purposes: a bleed air valve, which blew compressed air into the atmosphere, a cold air bypass, which diverted air from the compressor outlet to the post-combustor volume, and a hot air bypass, which was located at the heat exchangers outlet and bypassed the fuel cell emulator. Cold air valve, which was employed in this work, was observed to have a strong impact on cathode airflow, turbine inlet temperature, turbine speed, system pressures and surge margin. It was considered a critical actuator, because it is very effective in varying fuel cell temperature distribution. Hence, its complete characterization was considered fundamental for system control.

2. MODEL DESCRIPTION

The one-dimensional model simulates a planar, co-flow,

anode-supported SOFC. It employs a finite difference approach to solve the thermal equations and a finite volume approach for the electrochemistry. Details on the numerical model can be found in previous work [19]. Data are fed every 80 ms into the model from sensors embedded in the physical system. Distributed profiles of all the cell parameters (composition, temperatures, current density, overpotentials, and others) are calculated at each sample time. The model calculates in real-time the waste heat transferred to the turbine, as shown in Eq. 1, where h_{in} is the specific enthalpy change of the air at the cathode inlet, multiplied by cathode inlet airflow m_{in}, and h_{out} is the specific enthalpy change of the exhaust at the post-combustor outlet, where the unutilized fuel is burned, times the exhaust gas flow rate m_{out}.

$$\dot{Q} = \dot{m}_{out} h_{out} - \dot{m}_{in} h_{in} \quad \text{[kW]} \tag{1}$$

This value is then fed to a feedforward controller that commands a fuel valve. A fuel valve position is calculated in order to match the simulated heat transfer and the heat generated in the real combustor upstream the turbine.

During the test, the fuel valve was initially controlled by a PID to start up the turbine without the model in the loop. In the meantime, the model received real-time data from the sensors located at the volume inlet. When both the physical system and the numerical model reached the steady state and the fuel valve position calculated in the model matched the actual position, the model was connected switching the fuel valve controller from the PID to the feedforward model control.

When the model is in the loop, any change in the hardware system affects the fuel cell model, and any change in the model affects the hardware system. In this way it is possible to study the dynamics of the coupled system taking advantages from the model flexibility and ensuring high fidelity.

3. INSTRUMENTATION

Rotational Speed Measurement

Rotational speed is measured by an optical sensor, which picks up laser light reflected from a rotating target on the end of the generator shaft and transmits the pulse train to the frequency input of the control system. The optical sensor provides a 1,200 Hz signal at the nominal 40,500 rpm turbine speed with observed standard deviation in measurements of 50 rpm or 0.12% relative error in the precision of the measurement. The dynamic range of the speed variable is 1,000 to 50,000 rpm.

Compressor Inlet Flow

Compressor inlet flow is measured using an annubar flow element, which provides a mechanical average of the difference between stagnation pressure and static pressure in the inlet pipe to determine flow. Compressor inlet temperature and pressure reflect ambient conditions in the facility test cell during operation, and are used for calculating referred or corrected airflow and compressor pressure ratio. The time response is 300 ms.

Fuel Cell Simulator Flow

Primary airflow through the fuel cell simulator is measured at the entrance of the vessel using an annubar flow meter similar to the one at the compressor inlet. The combined temperature of the mixed streams from the heat exchangers is measured just upstream of the hot-air bypass valve. Pressure is also measured inside the air plenum of the fuel cell simulator.

4. RESULTS AND DISCUSSION

Two experiments were carried out moving the cold air bypass valve with a 15% step up from its nominal position. This value was chosen as the maximum step change allowed when the turbine speed is not controlled, in order to avoid damages to the turbine. The cold air valve bypasses the heat exchanger and the fuel cell volume, diverting air to the turbine inlet. In the first case (open loop) no control system was applied to the turbine speed, which was free to change, while in the second case (closed loop) the speed was kept constant by varying the turbine load. Each experiment was conducted three times to ensure reproducibility of the results. In both the experiments, the fuel valve was driven by the fuel cell model, simulating the heat transfer from the fuel cell system to the turbine. In order to keep constant turbine speed in the closed loop experiment, a load based speed controller was employed, which implementation was described in a previous work [12].

Nominal conditions of the system are illustrated in Table 1.

Table 1. Nominal system operating conditions

Turbine load	40 kW
Turbine speed	40,500 rpm
Pressure ratio	3.6
Compressor inlet flow	2 kg/s
Bleed air	1% of compressor inlet flow
Cold air	32% of compressor inlet flow
Hot air	2% of compressor inlet flow
Fuel cell load	220 A
Fuel utilization	70%
Anode fuel flow	0.1 kg/s
Cathode inlet flow	1 kg/s

The results showed the strong coupling between turbine speed, shown in Figure 2, and several other system parameters, such as cathode airflow and cell temperatures.

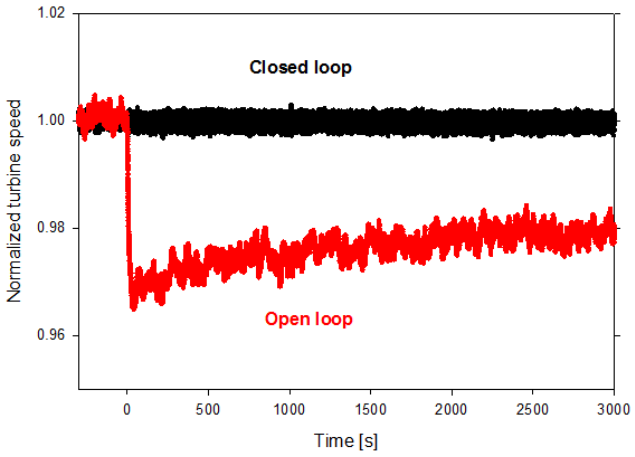

Figure 2. Turbine speed trend in open and closed loops

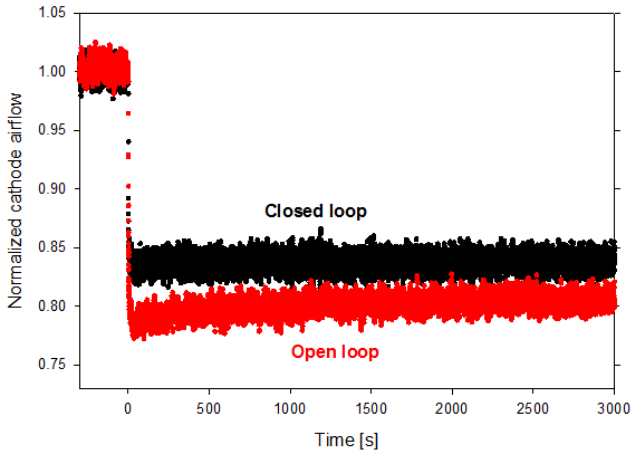

Figure 3. Cathode and bypass airflow trends in open and closed loops

After the bypass valve was opened, cathode airflow showed a significant reduction, as illustrated in Figure 3. When the turbine speed was free to change, the variation in cathode airflow was higher due to a self-propagating effect. The reduced turbine speed resulted in a lower compressor inlet airflow, as Figure 4 shows, causing a further reduction in cathode airflow. A 2% decrement in the turbine speed at steady state caused a 4% difference in cathode airflow compared with the closed loop scenario, when the speed was constant.

Turbine speed decreased in the first scenario because of two effects. First, the cold air diverted from the compressor discharge to the turbine inlet, bypassing heat exchangers and fuel cell emulator, caused a reduction in turbine inlet temperature (Fig. 5). In addition, a decrease in transferred heat from the fuel cell to the turbine was observed, as a consequence of a lower amount of cooling flow through the cell that caused more thermal energy to be stored in the cell, as explained later. This thermal effluent, shown in Fig. 6, is the only heating source of the system, driving the fuel valve in the combustor that simulates the fuel cell heat power. In closed loop, the decrement in turbine inlet temperature (TIT) and transferred heat was compensated by a PI controller, which imposed a lower electric load to the turbine in order to keep the speed constant.

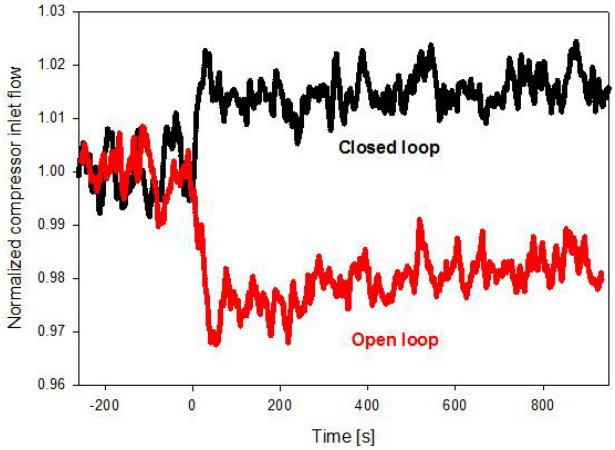

Figure 4. Compressor inlet mass flow trends in open and closed loops

Turbine inlet and outlet temperature trends in open loop and closed loop are presented in Figure 5. In open loop, the variation in TIT and TOT was about 3.5% of the nominal value, and the new steady state was reached after few minutes from the valve step change. The 2% reduction in compressed airflow, due to the lower turbine speed, resulted in a lower amount of bypassed air to the turbine compared with the closed loop case, and globally in a lower amount of airflow in the combustor. This was believed to mitigate, to some extent, the decrement in TIT. In closed loop a significant difference was observed in temperature trends. The immediate reduction in TIT was about 4%, and then the temperature kept decreasing gradually during time. Turbine outlet temperature decreased around 6%, following the same trend of TIT. The higher variation in closed loop compared with open loop was mainly due to the different compressor inlet mass flow, which increased of 2% in closed loop (Fig.4).

The thermal energy transferred to the turbine was very similar in both cases, as Figure 6 shows. In open loop, the decreased total airflow in the system after the speed reduction resulted in a higher temperature at the combustor exit. In addition, the amount of bypass flow increased around 26%, while in contrast, in closed loop the amount of airflow through the compressor increased slightly, and the increment in bypass flow was 32%. In both cases the bypass flow changed from 32% to 41% of the compressor inlet flow.

A larger variation of TOT than TIT in closed loop indicated that the efficiency of the turbine expander increased. The main cause was considered the reduction in turbine load to maintain constant speed. An increment in turbine inlet pressure was also believed to contribute, which was not observed in open loop where, in contrast, the inlet pressure decreased (Fig. 7).

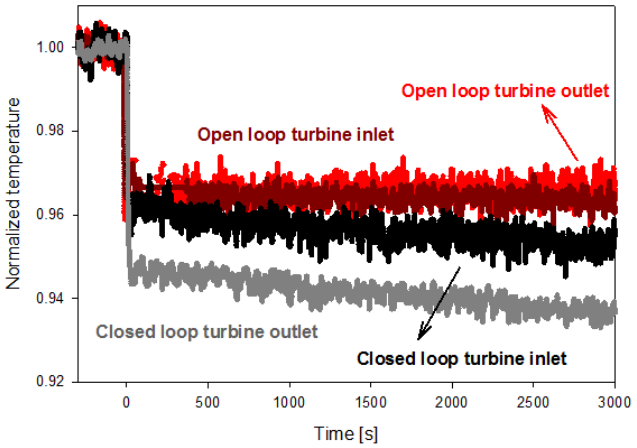

Figure 5. Turbine inlet and outlet temperature trends in open and closed loops

The heat transferred from the fuel cell to the turbine showed an initial reduction due to the lower cathode airflow, which caused a higher amount of generated heat to be stored in the fuel cell. Then it gradually recovered because the cathode inlet temperature decreased, as shown later in Fig. 9. As such, a reduction in air inlet temperature increased the temperature difference between airstream and fuel cell solid material, and consequently the heat transfer to the airflow after the initial decrement.

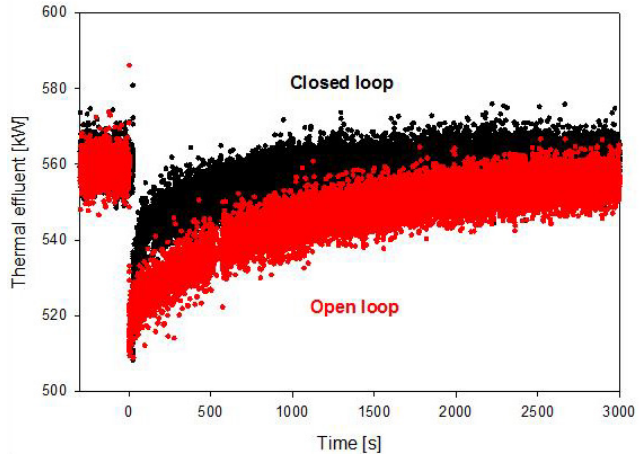

Figure 6. Heat transfer trends from the fuel cell system in open and closed loops

The pressure trends, presented in Figure 7, were significantly different in open loop and closed loop. In open loop both compressor discharge pressure and turbine inlet pressure decreased considerably, following the turbine speed trend. Turbine inlet pressure reduced about 2% less than compressor outlet pressure, because bypassing heat exchangers and additional volumes, the system pressure drop decreased significantly. In closed loop, compressor discharge pressure showed a small reduction because of the slight increment in compressor mass flow at constant speed. Also in this case the system pressure drop reduced due to the lower airflow through the recuperators and the volumes. Consequently, turbine inlet pressure increased. Pressure drops are presented in Figure 8.

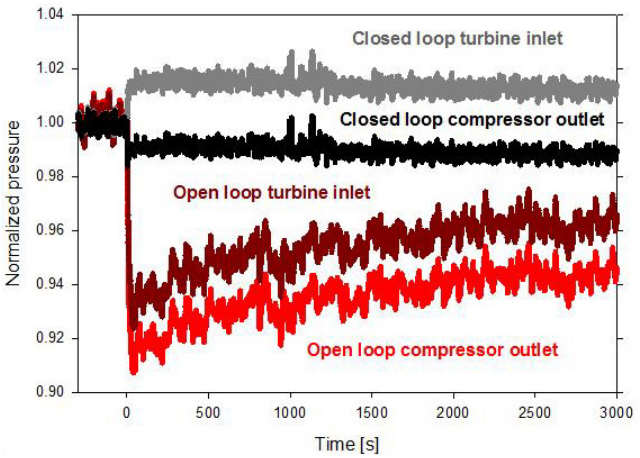

Figure 7. Pressure trends in open and closed loops

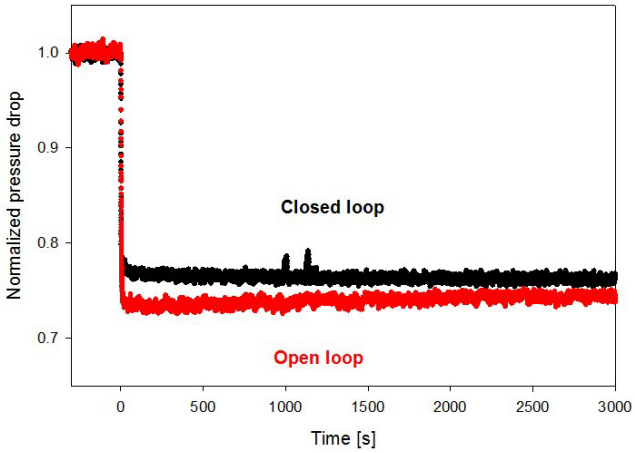

Figure 8. Pressure drop trends in open and closed loops

The air exiting the compressor was pre-heated with the turbine exhaust through two heat exchangers before feeding the cathode side of the cell. The significant decrement in TOT reduced the amount of heat transferred to the cold side of the recuperators, and this resulted in a lower cathode inlet temperature in both cases. In open loop, since the variation in TOT was smaller, cathode inlet temperature decreased about 12 °C, or 1.7% of the nominal value. In closed loop the variation was higher, and cathode inlet temperature reduced of 26 °C, or 3.5%. The trends are shown in Figure 9.

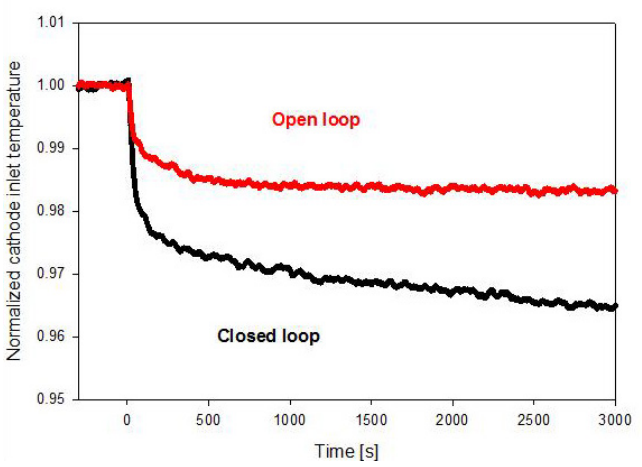

Figure 9. Cathode inlet temperature trends in open and closed loops

The difference in cathode inlet temperature mainly drove the different trends in cell average temperature, which was calculated as the mean value of the temperatures in the 20 nodes of the cell. In open loop the reduction in cathode airflow caused the average solid temperature in the cell to rise of 17 °C, around 2% of the initial temperature, as Figure 10 shows. In closed loop the temperature showed a different trend. The initial increment was significantly lower, less than 0.5%, and after 1000 seconds the temperature started decreasing again slowly.

After 3000 seconds, a scaling factor of 0.001 was applied to the cell heat capacity in order to reduce the fuel cell thermal capacity, accelerate the simulation, and evaluate the final steady state value. In open loop, the final temperature value was pretty close to the one at 3000 seconds, while in closed loop, the temperature showed a further decrement of 1% (8 °C) with respect to the initial steady state value. The closed loop behavior was mainly caused by the considerable reduction in cathode inlet temperature, which compensated the effect of the cooling flow decrease.

The reduced inlet temperature and cathode airflow caused in both cases a substantial increment in the temperature difference between cathode outlet and inlet, as Figure 11 shows. This difference can give an indication of the temperature gradients along the cell, which are not measurable but can induce detrimental stresses on the ceramic electrolyte if their value is too high. Hence, air temperature difference represents an important parameter for the control of the cell performance. As illustrated in Figure 11, the impact of cold air on ΔT was the same in closed loop and open loop by the time the new steady state was reached. Even though in closed loop both cathode inlet and outlet temperature were observed to be lower than in open loop, the increment in ΔT was in both cases around 20% (from approximately 170 °C to 205 °C).

This aspect is very important for the thermal management of the system. Normally, for large size systems, the turbine speed needs to be held constant if the system is connected to the grid, and this means that cold air bypass is not very effective in changing the average cell temperature. On the other hand, the impact on cathode inlet temperature and air ΔT across the cell was very high in both cases. This suggests that cold air bypass could be used in closed loop to mitigate ΔT variations without affecting the average temperature significantly.

In addition, ΔT response to airflow change was faster in closed loop, reaching the 63% of the new steady state value in half of the time compared with the open loop response. This was mainly due to the greater magnitude in cathode inlet temperature drop. The 63% criterion was considered for system identification and control research to identify the response time of different system parameters. The conclusion was that temperature difference could be controlled faster in closed loop if the cold air bypass was employed as actuator.

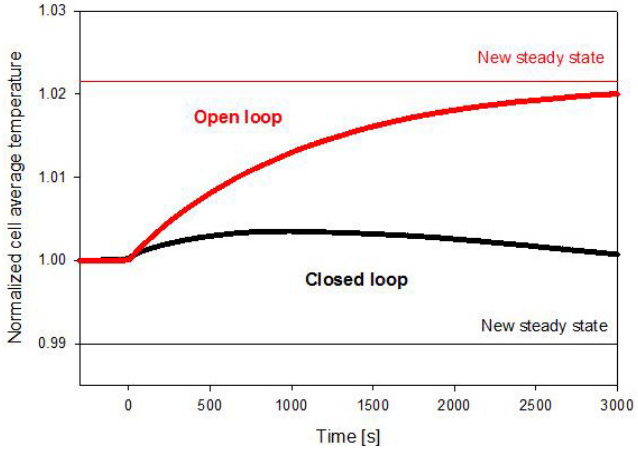

Figure 10. Average solid temperature trends in open and closed loops

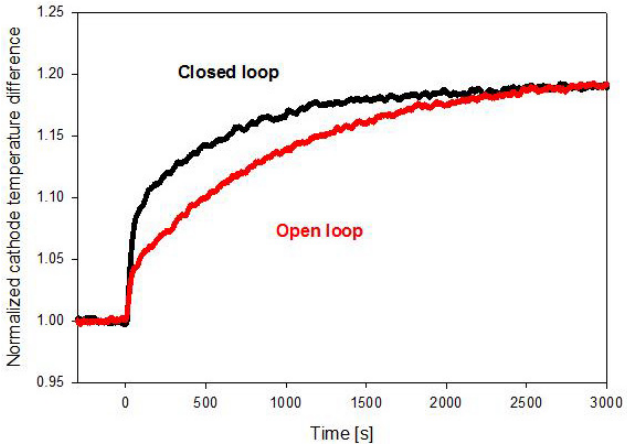

Figure 11. Cathode outlet-inlet temperature difference in open and closed loops

Another important aspect is the effect of cold air valve position on the surge margin. Surge margin was calculated as the shortest distance between the operative point and the surge line obtained from the compressor map. It depends on corrected compressor mass flow rate and operative pressure ratio, according with Equation 2. The numerical coefficients were found from the surge line on the compressor map.

$$SM = \left| \frac{\beta - 2.042\dot{m}_{nd} - 0.16}{\sqrt{1 + 2.042^2}} \right| \quad (2)$$

When the cold air valve was opened, surge margin increased in both cases. In open loop, a reduction in both compressor inlet mass flow and pressure ratio were observed due to the decrement in turbine speed. In closed loop, the operative point moved along the isovelocity curve while compressor inlet mass flow increased and the pressure ratio slightly decreased. The surge margin variation is presented in Figure 12, and it was comparable in the two cases. In both cases the reduction in system pressure drop due to the bypass of heat exchangers, fuel cell volume, and post combustor volume, was considered to contribute significantly to the surge margin increase.

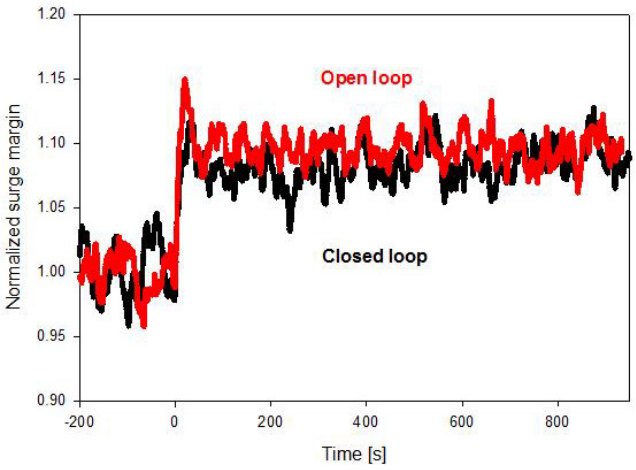

Figure 12. Surge margin trends in loop and closed loops

While the bleed air valve can provide a strong impact on surge margin, penalizing the efficiency of the system significantly, the cold air valve was considered an important actuator for long-term regulation of surge margin, since the bypassed air was still expanded into the turbine and the global efficiency was not affected as much.

5. CONCLUSIONS

The impact of cold air bypass variation on a fuel cell gas turbine hybrid system was analyzed comparing two different scenarios: open loop, where no control was applied to the turbine speed or the turbine inlet temperature, and closed loop, where the turbine speed was kept constant by varying the turbine load. Air was diverted from the compressor discharge to the turbine inlet, bypassing the heat exchangers and the fuel cell emulator.

Significant differences in the system parameter behavior was observed in the two cases, proving the strong coupling between cathode airflow and turbine speed in these systems. A variation in speed affected all the other variables in the open loop configuration, with a self-propagating effect. In particular, cathode airflow, system pressures, and average cell temperature showed stronger variations in open loop than in closed loop. In contrast, in closed loop cold air valve position affected cathode inlet temperature more significantly and ΔT across the fuel cell quicker than open loop cold air changes. Hence, the cold air valve could be very effective in regulating cell temperature difference without impacting the average cell temperature in a constant speed scenario.

Cold air valve also proved to be very effective in controlling the surge margin, in both cases. Thus, it is considered an important actuator for the safety of the system.

ACKNOWLEDGMENTS

This work was funded through the Crosscutting Research Program of the U.S. Department of Energy, National Energy Technology Laboratory (NETL) in Morgantown, WV. The work was supported in part by the NETL Research Participation Program, administrated by Oak Ridge Institute for Science and Education. The authors would also like to thank Dr. Paolo Pezzini from Ames Laboratory and Dr. Nor Farida Harun from McMaster University (Canada) for their valuable support.

REFERENCES

[1] Mueller F., Gaynord R., Auld A.E., Brouwer J., Jabbari F., and Samuelsen S., Synergistic integration of a gas turbine and solid oxide fuel cell for improved transient capability, *J. Power Sources*, 176, pp. 229–239, 2008.

[2] Veyo, S. E., Shockling, L. A., Dederer, J. T., Gillet, J. E., and Lundberg, W. L. Tubular Solid Oxide Fuel Cell/Gas Turbine Hybrid Cycle Power Systems: Status, *ASME J. Eng. Gas Turbines Power*, 124(4), pp. 845–849, 2002.

[3] Rao A.D., and Samuelsen G.S., Analysis strategies for tubular solid oxide fuel cell based hybrid systems, *Journal of Engineering for Gas Turbine and Power*, 2002, Vol. 124, pp. 503–509.

[4] Tucker D., Liese E., and Gemmen R., Determination of the Operating Envelope for a Direct Fired Fuel Cell Turbine Hybrid Using Hardware Based Simulation, *Proceedings of ICEPAG 2009 International Colloquium on Environmentally Preferred Advanced Power Generation*, 2009.

[5] Tucker D., Abreu-Sepulveda M., Harun N.F. SOFC lifetime assessment in gas turbine hybrid power systems, *Journal of Fuel Cell Science and Technology*, 2014, Vol. 11/051008, DOI: 10.1115/1.4028158.

[6] Liese E.A., Gemmen R.S., Jabbari F., and Brouwer J., Technical Development Issues and Dynamic Modeling of Gas Turbine and Fuel Cell Hybrid System, *ASME Paper 99-GT-360*, 1999.

[7] Ferrari M.L., Pascenti M., Bertone R., and Magistri L., Hybrid simulation facility based on commercial 100 kWe micro gas turbine, *Journal of Fuel Cell Science and Technology*, 2009, Vol. 6, 031008_1-8.

[8] Hohloch M., Widenhorn A., Lebküchner D., Panne T., and Aigner M., Micro gas turbine test rig for hybrid power plant application, *ASME Paper GT2008-50443*, 2008.

[9] Tucker D., Shelton M., and Manivannan A., The Role of Solid Oxide Fuel Cells in Advanced Hybrid Power Systems of the Future, *Interface*, 2009.

[10] Tucker D., Smith T.P., and Lawson L., Characterization of Bypass Control Methods in a Coal-based Fuel Cell Turbine Hybrid, *ICEPAG 2006-24008*, 2006.

[11] Pezzini P., Celestine S., Tucker D., Control impacts of cold-air bypass on pressurized fuel cell turbine hybrids, *Journal of Fuel Cell Science and Technology*, 2015, Vol. 12/011006, pp. 1-8, DOI: 10.1115/1.4029083.

[12] Pezzini P., Banta L., Traverso A., and Tucker D., Decentralized Control Strategy for Fuel Cell Turbine Hybrid Systems, *ISA Power Industry Division Symposium*, ISA-PWID2014-52, 2014.

[13] Zhou N., Yang C., and Tucker D., Evaluation of cathode air flow transients in a SOFC/GT hybrid system using hardware in the loop simulation, *Journal of Fuel Cell Science and Technology*, 2015, Vol. 12/011003, DOI: 10.1115/1.4028950.

[14] Zhou N., Yang C., and Tucker D., Evaluation of Compressor Bleed Air Transients in a Fuel Cell Gas Turbine Hybrid System Using Hardware Simulation, *Proceedings of ASME Turbo Expo 2015*, Montreal, Canada.

[15] Inui Y., Ito N., Nakajima T., and Urata A., Analytical Investigation on Cell Temperature Control Method of Planar Solid Oxide Fuel Cell, *Energy Conversion and Management*, 2006, Vol. 47, pp. 2319-1328.

[16] Traverso A., Magistri L., and Massardo A.F., Turbomachinery for Air Management and Energy Recovery in Fuel Cell Gas Turbine Hybrid Systems, *Energy*, 2010, Vol. 35, pp. 764-777.

[17] Zhou N., Yang C., Tucker D., Pezzini P., and Traverso A., Transfer Function Development for Control of Cathode Airflow Transients in Fuel Cell Gas Turbine Hybrid Systems, *International Journal of Hydrogen Energy*, 40(4):1967-1979, 2014.

[18] Traverso A., Tucker D., and Haynes C., Preliminary Experimental Results of Integrated Gasification Fuel Cell Operation using Hardware Simulation, *Journal of Engineering for Gas Turbine and Power*, 2012, Vol. 134, pp. 071701/1-10.

[19] Hughes D., Wepfer W.J., Davies K., Ford J.C., Haynes C., and Tucker D., A Real-Time Spatial SOFC Model for Hardware-Based Simulation of Hybrid Systems, *ASME 2011 9th International Conference on Fuel Cell Science, Engineering and Technology*, 2011.